EAGLE INTERNAL NOTE :
CAL-NO-005
6 NOVEMBER 1991

CAN WE PREDICT RADIATION LEVELS IN CALORIMETERS?

A. Ferrari, P.R. Sala
Istituto Nazionale di Fisica Nucleare INFN,
Sez. di Milano, Via Celoria 16, 20133 Milano
and
A. Fassò, G.R. Stevenson
CERN, Geneva, Switzerland

ABSTRACT

A description is given of radiation level simulations for LHC and SSC detectors. The various sources of uncertainty are analyzed and discussed. It is shown that relative comparison can be made at the 10 % level provided suitable simulation tools are used: however absolute values can be trusted only within a factor 2 due to systematic errors deriving mainly from the source term. Results for neutron fluxes and doses for geometries inspirated to the EAGLE detector for LHC and to SDC for SSC are presented.

1. Introduction

The construction of the next generation of colliders and of the associated detectors will require large efforts in many fields. The high intensity required by the physical goals will put severe constraints both on machine and detector components. Radiation damage can greatly influence any technical choice and therefore reliable and detailed predictions about radiation levels are mandatory. In the following sections simulations tools used for computing the radiation levels expected for the LHC and SSC detectors are briefly analyzed: an indication of their accuracy and reliability is given. The source data used for p-p inelastic interactions at $\sqrt{s} = 16, 40$ TeV and their implications on the final results are discussed in section 3.

The last sections present detailed estimates both of neutron fluxes and doses arising from ionizing particles in realistic detector geometries for LHC and SSC. The influence of many parameters on these quantities and the possibility of minimizing the radiation levels with a careful choice of some of them are also discussed.

2. The FLUKA code

The FLUKA code has been widely used at CERN for shielding and radiation protection calculations. It has recently undergone substantial improvements as described in table 1. All the calculations presented in the following have been performed using the last version (FLUKAN) of the code. Details can be found in refs.[1,2] for FLUKA86, and in refs.[3-6] for the improvements. We discuss only the low energy neutron transport part, since it is the most relevant for the present calculations.

2.1 Transport of Low Energy Neutrons ($E_n < 20$ MeV)

Table 1
Short description of the original FLUKA code and its present version FLUKAN

Topics	FLUKA86	FLUKAN
Hadron- nucleus interactions, 5-10 GeV/c < p < ≈ 10TeV , primary interactions	Dual Parton Model (NUCEVT, HADEVT, BAMJET)	Removed known bugs and approximations
Hadron- nucleus interactions, 50 MeV < E < 5GeV , primary interactions	NUCRIN: resonances production (HADRIN) and their decay (DECAY)	Modified versions of HADRIN/NUCRIN, preequilibrium reactions below 200 MeV for p and n
Cascade following primary interactions	Parametrized	Strongly modified: correlation of cascade with primary int., nuclear effects taken into account
Nuclear de-excitation	None	Particle evaporation with a modified version of EVAP-5 followed by γ de-excitation
Stopping $\bar{p}$, $\bar{n}$, π^-	On spot energy deposition or decay	$\bar{p}$, $\bar{n}$ treated by NUCRIN,π^- by preequilibrium
Hadrons below 50 MeV	On spot energy deposition or decay	Protons: nuclear reactions plus dE/dx ;other charged hadrons: dE/dx; neutrons: reactions above 20 MeV, specialized treatment below; other neutrals: transported till decay.
Electromagnetic shower	EGS4	Electron transport completely modified. New treatment of photoelectric effect and of bremsstrahlung (LPM effect included)
Geometry	Combinatorial	New bodies, optimization with strong speed up factors. Tranport in magnetic field
Biasing	Leading particle biasing	Leading particle biasing, region importance biasing, russian roulette and splitting for secondaries production. Biased downscattering and non-analogue absorption for low-energy neutrons. All region dependent
Time analysis	None	Complete

The treatment of neutron interactions in this energy range is based on data sets

containing all relevant information: this approach is possible since there are large and accurate compilations of nuclear data for neutrons. This highly specialized part of FLUKA is similar to the transport part of the MORSE code[7]: however so many modifications were required that a set of new routines have been written instead of using the original ones from MORSE. It is sufficient to say that energy and direction of neutrons are selected according to appropriate downscattering matrices taking into account all relevant reaction channels.

The most important items are the cross section data sets. Data compilations must be processed to produce suitable input files for transport codes: generally available processed data sets are usually limited to a few materials and often they do not contain all informations. To overcome these problems a collaboration was started with the ENEA laboratory specialized in nuclear data processing for reactor and fusion applications. This led to the production of a data set especially tuned for detector and machine application for high energy colliders[8]. It contains data for about 40 elements using 72 neutron energy groups: whenever available gamma ray generation data have been included. Partial reaction cross sections and kerma factors are also included. The Doppler broadening fo cross section resonances has been taken into account processing a few materials not only at room temperature, but also at 87° K (Liquid Argon temperature) and at 0° K (that means no Doppler broadening), which is suitable for liquid helium cooled apparatus.

2.2 Code Validation

Many tests of the new version of the code have been performed. Only a few of them will be discussed here: they mainly concern the hadronic part since for the present problem the modifications made to EGS4 are not believed to be important.

The inelastic event generator has been tested comparing its predictions against experimental data for rapidity distributions, shower, grey and black particle average multiplicities and multiplicity distributions over a wide range of energies up to 800 GeV and for a large variety of target nuclei. The agreement with the experimental data is generally good: the results obtained for grey and black particles made us confident that the modifications to the cascade and evaporation parts are correct and reliable. An example is shown in fig.1.

Much care has been put in testing the new module for nucleon-nucleus interaction below 200 MeV. The agreement with experiments is satisfactory and it is apparent that this module represents a substantial improvement in this energy range: these tests are very important for neutron transport calculations due to the large number of medium-low energy neutrons in a hadronic cascade. An example is presented in fig.2.

A very important test which can directly give informations on code reliability in predicting hadronic cascades can be found in ref.[11]. It was shown that the new version of FLUKA is usually in good agreement with experimental data in predicting neutron fluxes produced by 24 and 200 GeV proton beams on Iron and Lead dumps[12]. The code successfully predicts both the radial and longitudinal

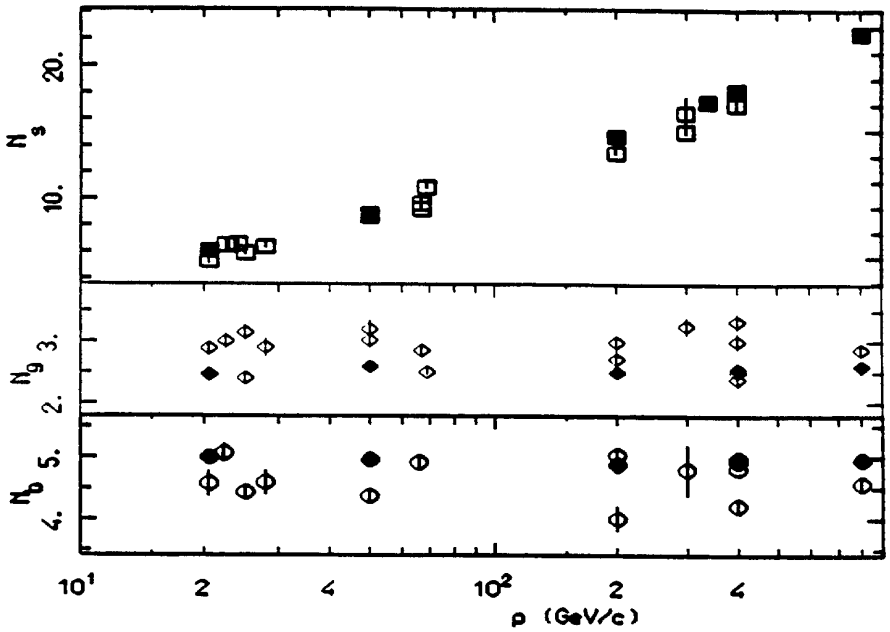

Fig. 1 : Average multiplicities of charged black(N_b), grey (N_g) and shower(N_s) particles produced by protons of different energies in emulsions. Full symbols are FLUKAN results, open symbols are experimental data[9]

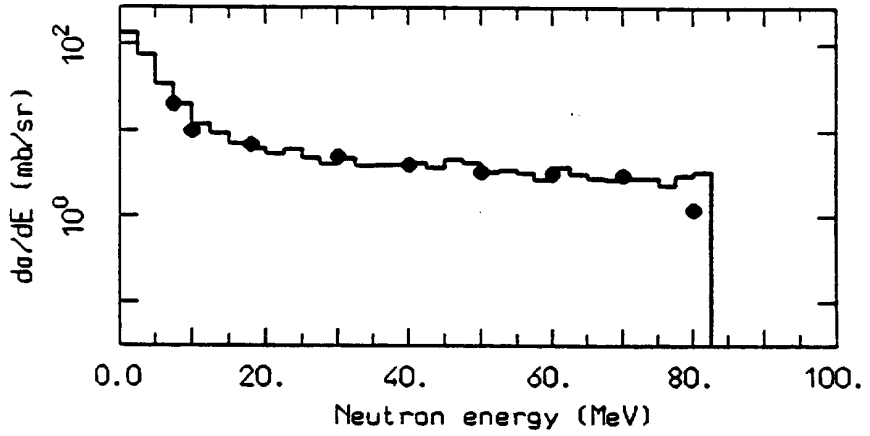

Fig. 2 : Neutron spectrum following bombardment of ^{58}Ni nuclei with 90 MeV protons. Points are experimental data[10]

distribution of the flux measured by different activation detectors with threshold as low as 1 MeV: the agreement for albedo neutrons is also good. Preliminary comparisons[11] show also nice agreement with doses measured with RPL glasses in the same experiments. These benchmarks make us confident that FLUKAN predictions can usually be trusted within the uncertainties of neutron dosimetry (which can be estimated of the order of 10-20 %).

3. The Source Term

Any calculation on the radiation levels in future detectors requires specific assumptions on the number, identity and spectra of particles emitted in minimum bias events. However due to the lack of experimental data, it is necessary to use physical models whose reliability at the energy of interest can be a major source of uncertainty in the final result. For all calculations presented in the next sections primary p-p events were generated using the DTUJET90 code[13]. A full description of the physics model underlying this code can be found in the original papers: we want only to stress that the code includes all processes relevant for the prsent task, and it is in nice agreement with experimental data up to the Tevatron energy. The properties of the events generated by DTUJET are summarized in table 2, for $\sqrt{s}$ = 16 and 40 TeV. However the reader must keep in mind that these events were generated using a standard set of structure functions: other sets can give different results. The uncertainty introduced can be quite large: events generated with "extreme" structure functions[14] resulted in a 50 % increase of the multiplicity as illustrated in table 2. Unfortunately no discrimination can be made on the basis of available experimental data since both sets go into the same results approaching the present collider energies. A few exploratory runs were also performed using a different code[15] for generating primary events, however the resulting differences in the final results are well within the uncertainties discussed above and therefore they do not justify any further effort in this direction.

Finally it must be mentioned that, for a given luminosity, a 10-20 % scale error derives from the uncertainties on the inelastic cross section adopted for p-p collisions.

4. Radiation Environment for a Realistic LHC Detector

In the following the results of simulations carried out for a realistic LHC detector configuration are presented. The quantities scored are neutron spectra and doses due to ionizing particles in the various parts of the detector.

4.1 General Considerations and Assumptions

The detector geometry used for these calculations is presented in figure 3: the surfaces and volumes used for scoring neutron fluxes are also indicated. The main features of this geometry, taken from a simple sketch of the EAGLE collaboration, are presented in table 3. The Barrel Calorimeter covers down to η = 2, while the End Cap one goes down to η = 3. The materials of the Electromagnetic and Hadronic Calorimeters have been treated like homogeneous mixtures of the proper amounts of absorber and active media. This approximation does not cause any significant consequence on neutron fluxes calculations, since neutron mean free paths are larger than the typical dimensions of calorimeter cells. On the contrary this is surely an approximation for doses: the proper dose to an active material should be computed multiplying for the ratio between its mass stopping power and

Table 2
Mean properties of secondaries generated in p-p events by the DTUJET code

LHC, 'standard' structure functions

	Multiplicity					Mean p_T (GeV/c)				
η	Tot.	Ch.	π^0	γ	Str.	Tot.	Ch.	π^0	γ	Str.
0.- 2.	45.	25.	13.	1.1	5.9	0.46	0.46	0.39	0.36	0.67
2.-4.	50.	28.	13.	1.1	8.0	0.43	0.42	0.36	0.38	0.57
2.-6.	39.	22.	10.	0.8	6.5	0.41	0.40	0.36	0.37	0.53
2.-8.	23.	13.	6.1	0.5	3.8	0.38	0.37	0.33	0.32	0.48
2.-10.	8.0	4.7	1.9	0.1	1.2	0.30	0.29	0.25	0.28	0.36
10.-∞	0.7	0.4	0.1	0.01	0.08	0.14	0.14	0.11	0.14	0.14
0.-∞	165.	93.	45.	3.7	26.	0.42	0.41	0.36	0.36	0.56

LHC, 'extreme' structure functions

	Multiplicity					Mean p_T (GeV/c)				
η	Tot.	Ch.	π^0	γ	Str.	Tot.	Ch.	π^0	γ	Str.
0.-2.	71.	41.	21.	1.9	9.1	0.46	0.46	0.38	0.35	0.66
2.-4.	75.	42.	20.	1.8	12.	0.42	0.41	0.36	0.35	0.56
2.-6.	57.	32.	15.	1.3	9.4	0.40	0.40	0.35	0.35	0.52
2.-8.	29.	16.	7.3	0.6	4.9	0.35	0.34	0.30	0.32	0.43
2.-10.	8.2	4.7	1.9	0.1	1.3	0.27	0.27	0.23	0.25	0.31
10.-∞	8.2	4.7	1.9	0.1	1.3	0.12	0.12	0.10	0.05	0.12
0.-∞	241.	136.	66.	5.7	37.	0.41	0.41	0.35	0.34	0.54

SSC

	Multiplicity					Mean p_T (GeV/c)				
η	Tot.	Ch.	π^0	γ	Str.	Tot.	Ch.	π^0	γ	Str.
0.- 2.	48.	27.	14.	1.3	6.4	0.47	0.46	0.40	0.36	0.67
2.-4.	52.	29.	14.	1.2	8.7	0.43	0.42	0.37	0.38	0.56
2.-6.	43.	24.	11.	0.9	7.2	0.42	0.42	0.36	0.35	0.54
2.-8.	29.	16.	7.6	0.6	4.8	0.41	0.41	0.35	0.39	0.53
2.-10.	14.	7.9	3.5	0.2	2.1	0.35	0.35	0.29	0.33	0.43
10.-∞	2.8	1.7	0.6	0.03	0.5	0.22	0.22	0.19	0.15	0.26
0.-∞	189.	106.	51.	4.2	30.	0.42	0.42	0.36	0.36	0.56

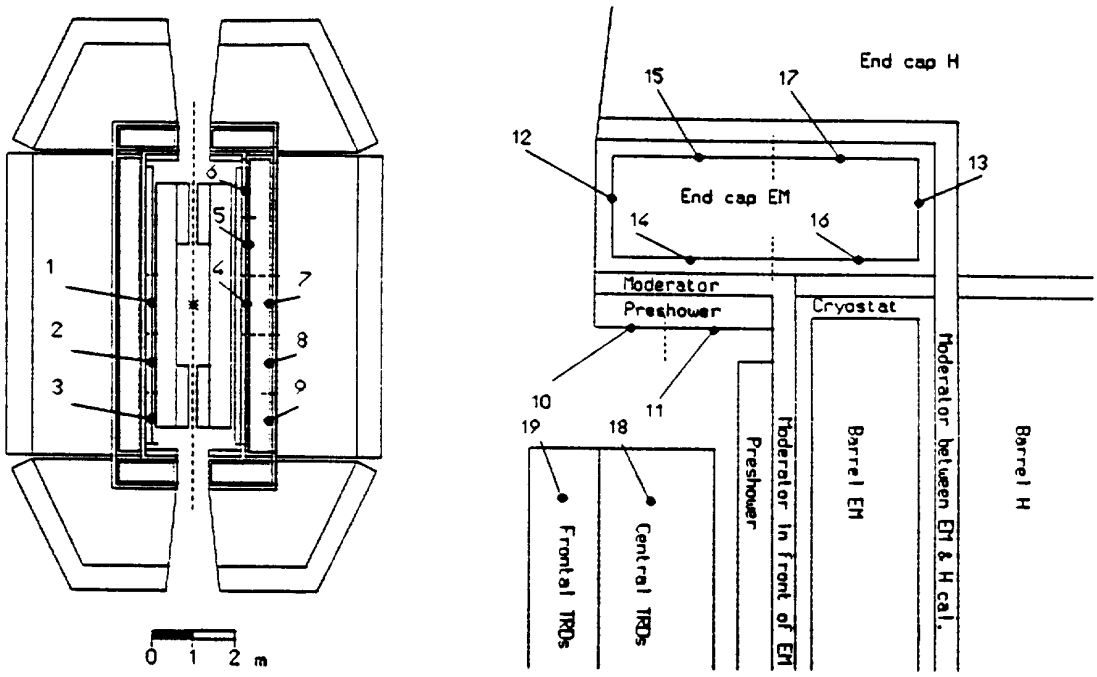

Fig. 3 : Geometry and scoring surfaces used in calculations for a LHC detector: Horizontal section (left) and magnification of the End Cap zone (right)

that of the homogeneous medium. Moreover, such a procedure can be incorrect if the material considered significantly perturbs the radiation spectrum. Therefore, a correct computation can be made only knowing both the geometry and composition of the zone of interest and the surrounding media (which is not trivial for example for a preamplifier). For this reason, and since mass stopping power ratios are always not much different from one , in the following we report doses to the "average" materials without any corrections.

The results of the calculations have been converted to annual doses and fluxes assuming an inelastic cross section $\sigma_{in} = 60$ mb and an integrated luminosity $L = 10^{41} cm^{-2}$ corresponding to a luminosity of $10^{34} cm^{-2} s^{-1}$ and a beam time of $10^{7} s$. The cross section does not include single diffractive events which have been removed from the file generated with DTUJET90. Due to the considerations outlined in section 3, there is a systematic uncertainty arising from the source term alone which is at least of the order of 50 %. The systematic errors introduced by the whole cascading process are estimated to be of the order of 20 % for neutrons, according to the discussion of section 2.2, while are likely to be smaller for doses. Bearing in mind these systematic effects and taking into account that they are rather independent from the considered configuration, the results presented in the following can be compared at the 5-10 % level corresponding to the typical statistical errors of the calculations. Every configuration has been tested with 300 primary p-p events randomly choosen out of a set of 850. These figures should be large enough

Table 3
Possible configurations for a LHC detector considered in this work

Config.	Description
1	Reference Configuration. Barrel: Lead-LAr EM cal. (R_{min}=125cm, -2 < η <2), Iron-LAr H cal. . End Cap: Lead-LAr EM cal. (-3 < η <3), Iron-LAr H cal. . Magnetic Field: 2 T solenoidal field (-2 < η <2, R <115 cm). No moderator, no TRD in the central cavity.
2	Same as 1 but without magnetic field
3	Same as 1 but with a Lead-LAr hadronic calorimeter instead of the Iron-LAr one
4	Same as 1 but with an Iron-Scintillator hadronic calorimeter instead of the Iron-LAr one
5	Same as 1 but with an Iron-Scintillator hadronic calorimeter instead of the Iron-LAr one and a Lead-Scintillator EM calorimeter instead of the Lead-LAr one.
6	Same as 1 but with a 10 cm polyethylene layer all around the EM calorimeter entrance face, both on the Barrel and the End Cap.
7	Same as 1 but with a 10 cm polyethylene layer between the EM calorimeter and the H one.
8	Same as 1 but with Transition Radiation Detectors (TRD) in the central cavity: the assemblies of both lateral and frontal TRDs are simulated as a proper amount of hydrogenated material uniformly distributed over the volume occupied by TRDs (see fig. 3).
9	Same as 1 but with a 10 cm polyethylene layer in front of the End Cap EM calorimeter only.
10	Same as 1 but with a 10 cm polyethylene layer in front of the End Cap EM calorimeter only and the TRDs in the central cavity (it is a combination of configurations 8 and 9).
11	Same as 1 but with the End Cap covering now down to η=4.
12	Same as 1 but with the End Cap covering now down to η=4 and with TRDs in the central cavity (Configurations 8 and 11).

to avoid any selection effect. To save CPU time during neutron flux calculations, electrons, positrons, gammas and π^o have been immediately discarded, so neglecting the small contribution deriving from photohadron interactions.

4.2 Neutron Fluxes

The effects of the magnetic field, of different materials for the EM and Hadronic Calorimeters, of moderating materials inside the central cavity and of different forward cone apertures on neutron fluxes have been investigated and are presented in the following.

It is customary to present neutron fluxes with a threshold set at 100 keV, which roughly corresponds to the threshold for damaging silicon based semiconductors[16] or also to normalize the fluxes assuming a unit damage for 1 MeV neutrons and folding the spectrum with the silicon damage function. However there is a growing interest in the use of GaAs based devices such as preamplifiers, both for their radiation hardness and intrinsic electronic properties: the damage function of GaAs[17] is quite

different from that of silicon, and presents a non negligible sensitivity down to thermal energies. We decided therefore to present the data on neutron fluxes both with and without the 100 keV threshold, however the discussion in the following paragraphs and the comparisons between different configurations are restricted to fluxes with $E_n > 100$ keV to avoid confusion. Most of the conclusions are at least qualitatively the same also for the total flux.

4.2.1 Reference Configuration

To discuss the effect of the various modifications, the configuration described in table 3, point 1, has been assumed as the reference one. It is a possible configuration for the EAGLE detector without any moderating material and with a 2 T solenoidal magnetic field inside the central cavity (no field in the EM and Hadronic calorimeters). The EM calorimeter is made of Lead-Liquid Argon (LAr), and the hadronic one of Iron-LAr, with appropriate partial densities. Preshower detectors are placed in front of both the Barrel and the End Cap EM Calorimeters, and an aluminium cryostat, which can also mimic the effect of the coils, is considered. The results of table 4, 5 show that neutron fluxes will range roughly from $2\text{x}10^{13} n/cm^2/yr$ at the barrel entrance to 10^{14} in the most exposed End Cap positions for such a configuration.

4.2.2 Modified Configurations

The results for a few configurations both for the flux above 100 keV and the total flux are presented in table 4. The positions where neutrons have been scored can be seen in fig. 3. It must be noted that in the configurations 11 and 12 the scoring surfaces 12,14,15 are actually at inner positions since they have been moved down to $\eta = 4$.

Table 5 presents a direct comparison among all configurations for a few selected points: only neutrons with $E_n > 100\ keV$ have been considered here. Differences smaller than 10 % have been omitted since they are not statistically significant, of course caution must be used in interpreting variations close to that limit. In the last years many estimates of the expected radiation environment for the LHC detectors have been published in the literature[18]. Most of them combined simple analytical models with Monte Carlo simulations in idealized geometries to derive the quantities of interest. A comparison of our results with these estimates is rather difficult and position and configuration dependent. Such a comparison in a simpler geometry has been done in ref.[19]. Here the reader can find both a detailed discussion and the hint that there are positions/configurations where significant differences can arise.

4.2.3 Effect of the Magnetic Field

The 2 Tesla magnetic field has only a minor effect on the neutron fluxes: this is not unexpected since such a field with a Barrel radius of 1.2 m cannot bend enough charged particles to prevent them from impinging on the Barrel.

4.2.4 Effect of Different Materials for the Calorimeters

Table 4

Neutron fluxes in EAGLE (in unit of 10^{13} neutrons/cm^2/yr). First line: flux with $E_n > 100$ keV. Second line: total flux. Values with statistical errors greater than 20% are marked with an asterisk

Posit.	Configurations											
	1	2	3	4	5	6	7	8	9	10	11	12
1	1.7	2.0	2.7	1.5	.84	.17	1.6	.41	1.1	.44	3.1	.47
	6.9	9.4	9.6*	4.3	2.7*	.37	3.4	1.9*	3.7	1.3	14.	2.5
2	2.0	2.2	3.0	1.7	.99	.26	1.8	.58	1.1	.50	3.6	.76
	7.4	11.	11.	4.5	3.1*	.50	3.5	3.0*	3.5	1.6	15.	3.2
3	3.2	3.5	5.0	2.7	1.6	.41	2.7	2.1	1.3	.92	6.0	3.6
	10.	14.	16.*	6.9	4.3	1.1*	5.2	12.*	3.7	2.6	26.	12.
4	1.1	1.5	1.6	.99	.39	.47	1.1	.66	1.0	.77	1.6	.69
	5.7	8.3	7.6*	3.4	.99	.89	2.4	1.7	3.5	1.7	12.	2.3
5	1.2	1.7	1.8	1.1	.46	.49	1.2	.85	1.1	.87	1.9	.93
	5.9	9.7	9.0*	3.7	1.1	1.0	2.7	2.6	3.5	2.2	11.	3.6
6	1.7	2.2	2.8	1.6	.70	.57	1.7	1.7	1.1	1.1	3.0	2.3
	8.1	10.	12.*	5.2	1.8	1.5	3.7	8.4*	3.2	2.6	18.	8.5
7	.72	.77	1.1	.62	.04	.43	.52	.46	.60	.53	1.0	.52
	4.5	5.3	5.3	2.9	.08	1.1	1.4	1.3	2.1	1.3	8.7	2.1
8	.77	.88	1.1	.72	.04	.40	.64	.57	.60	.58	1.1	.68
	4.8	5.6	5.4*	3.2	.10	1.1	1.6	3.1*	2.2	1.6	11.	3.1
9	1.0	1.0	1.6	.94	.04	.46	.80	.79	.63	.70	1.7	1.3
	6.5	5.4	7.6	4.1	.09	1.5	2.0	6.4*	1.8	1.8	16.	7.0
10	6.0	6.7	9.9	5.2	4.4	1.6	5.1	5.3	2.6	2.3	18.	14.
	16.	20.	30.*	11.	8.8	3.3	9.0	16.	5.6	5.1	46.	29.
11	3.2	3.7	4.8	2.9	1.7	.27	2.9	2.9	.84	.72	6.2	4.9
	9.9	13.	18.*	6.7	3.5	1.3*	5.3	13.*	2.4	2.1	24.	14.
12	15.	15.	26.	13.	12.	15.	12.	16.	14.	17.	55.	46.
	28.	34.	46.	19.	27.	25.	18.	29.	23.	29.	99.	65.
13	1.7	1.2	3.5	1.3	.05	1.1	1.0	1.2	.93	1.1	2.7	2.3
	7.8	7.4	10.	4.6	.12	4.5	2.3	5.9	2.7	3.0	18.	12.
14	8.5	8.1	14.	7.4	4.1	7.2	7.4	8.4	7.3	8.4	43.	35.
	19.	22.	27.	13.	8.4	15.	11.	24.*	14.	15.	78.	53.
15	9.6	11.	22.	8.1	3.3	9.8	6.8	12.	10.	12.	56.	44.
	22.	33.*	45.*	14.	8.5	19.	11.	38.*	20.	25.	108.	66.
16	2.8	2.7	5.1	2.5	.44	2.0	2.2	2.5	1.7	2.0	4.9	4.1
	9.9	11.	14.	6.3	1.1	5.5	4.3	9.3	4.0	4.5	23.	15.
17	2.8	3.0	7.3	2.4	.32	2.7	1.9	2.9	2.7	3.0	4.9	4.2
	9.8	11.	22.*	6.1	.87	7.8	3.6	10.*	6.7	8.3	23.	14.
18	2.1	2.4	3.2	1.8	1.0	.26	1.9	.60	1.1	.42	4.0	.86
	7.6	10.	13.	4.8	2.6	.54	3.7	3.9	3.5	1.8	17.	4.2
19	2.4	3.0	4.1	2.1	1.3	.40	2.2	.92	1.3	.63	5.0	1.5
	8.7	11.	13.	5.2	3.0	.70	4.3	3.9	3.5	2.3	21.	6.7

Table 5

Neutron fluxes in the configurations listed in table 3: The first line shows the fluxes concerning the reference configuration, while in the following lines the percentage difference with respect to line 1 is reported for a selected set of positions (see fig.3). Differences smaller than 10% have been omitted. Only neutrons with $E_n > 100$ keV have been included.

Config.	Positions						
	Barrel			End Cap			η_{max}
	1 p.s.	4 EM in	7 EM/H	10 p.s.	14 EM in	15 EM/H	12 EM in
1	1.7E+13	1.1E+13	7.2E+12	6.0E+13	8.5E+13	9.6E+13	1.5E+14
2	+ 17 %	+ 47 %	=	+ 12 %	=	+ 15 %	=
3	+ 56 %	+ 52 %	+ 54 %	+ 66 %	+ 64 %	+130 %	+ 77 %
4	- 13 %	=	- 14 %	- 12 %	- 13 %	- 16 %	- 13 %
5	- 51 %	- 63 %	- 95 %	- 26 %	- 52 %	- 65 %	- 15 %
6	- 90 %	- 56 %	- 40 %	- 73 %	- 15 %	=	=
7	=	=	- 28 %	- 14 %	- 13 %	- 29 %	- 16 %
8	- 76 %	- 37 %	- 36 %	- 12 %	=	+ 26 %	=
9	- 37 %	=	- 17 %	- 57 %	- 14 %	=	=
10	- 74 %	- 27 %	- 27 %	- 61 %	=	+ 29 %	+ 18 %
11	+ 83 %	+ 49 %	+ 40 %	+196 %	+407 %	+489 %	+280 %
12	- 73 %	- 34 %	- 28 %	+130 %	+318 %	+357 %	+219 %

The replacement of iron with lead as absorber in the hadronic calorimeter causes a significant increase in the neutron fluxes, ranging from 1.5 on the preshower up to 2 at the transition between the EM and H calorimeters. Only a slight reduction arises from the use of an Iron-Scintillator hadronic calorimeter despite its larger moderating power with respect to Fe-LAr. Larger effects are obtained using scintillators as active media also for the EM calorimeter. They are larger inside the barrel than on its internal surface, showing that neutron fluxes on the Barrel are dominated by low energy neutrons multiscattered in the central cavity and not by neutrons originating from interactions in the Barrel itself (see also ref.19 about this problem).

4.2.5 Effect of Moderators

The above conclusion is strongly supported by the results of the run with a 10 cm polyethylene layer in front of the EM calorimeter. It is apparent that all positions benefit from that layer up to a factor of ten, which could be explained only if fluxes were mainly due to neutrons multiscattered in the central cavity, rather than locally produced by inelastic interactions. The relative insensitivity of position 14,12 can be explained remarking that at high rapidities the contribution of locally produced neutrons is surely more important and also that no polyethylene

was placed on the End Cap side directly facing the central cavity (surface 12 of fig. 3): the possibility of placing such a layer must be further investigated since it is likely that the benefits can be more than compensated by the unwanted extra amount of interactions due to the restriction of the forward cone. It must be stressed that the presence of such layer in front of the Barrel EM has so many drawbacks on its performances that it can be excluded a priori at least in this crude form. Configuration 6 must therefore be regarded as an useful exercise rather than a realistic ansatz to reduce the neutron problem. A further attempt can be to move the moderating layer beyond the EM calorimeter: this was done with Config. 7, however the resulting reductions are very discouraging. Unlike the polyethylene layer of Config. 6 the situation described in Config. 8 is realistic and shows how also minor structures can have important effects. Since it has been proposed to use assemblies of Transition Radiation Detectors (TRD) and they would contain a certain amount of hydrogenated material, their presence was schematized as a uniform region of polyethylene of appropriate density (regions 18,19 in fig. 3) in the central cavity. Rather surprinsingly, despite the integrated radial thickness is only about 3 cm, they resulted in a significant reduction of the neutron flux on the Barrel, maybe because of the large solid angle covered by such assembly and the long paths that neutrons coming from the End Cap regions must cross in it. The next step still exploits a polyethylene layer but this time limited to the End Cap region only, where it could be accepted by physicists. The goal is to try to decouple neutrons coming from the large η regions from the Barrel. A certain reduction is achieved but of course it is smaller than the one of Config. 6. Combining such a limited polyethylene shield with the TRDs gives the results shown for Config. 10. It can be seen that significant reductions can be achieved both on the Barrel and on the End Cap preshowers: however no reduction occurs in the End Cap EM part most exposed to radiation, and there are indeed indications that a slight increase can occur in pos. 12, probably due to interactions occuring in the frontal part of the TRDs assembly which extends down to 10 cm from the beam axis.

4.2.6 Effect of the Forward Cone Aperture

A test has been made with the same geometry but with an $\eta = 4$ forward cone. The flux increase is quite large, especially on the End Cap as expected, but also the Barrel regions are affected. However if we introduce the TRDs (config. 12) we can reach again the same fluxes on the Barrel EM and preshowers as with the $\eta = 3$ End Cap. This result strongly suggests that if a suitable technology will be available to build an End Cap Calorimeter covering down to $\eta = 4$ which can survive to these radiation levels, no significant consequence will occur at the Barrel Calorimeters provided an appropriate amount of hydrogenated material is present in any form in the central cavity.

4.3 Dose rates

Dose rates are mainly dominated by the electromagnetic component of the

cascades. As a consequence they are much less dependent on details like the presence of moderating materials or the exact composition of the EM and H Calorimeter, provided the absorber material in the EM Calorimeter is the same.

Due to the reasons explained above, only few configuration have been run for doses, checking mainly the effect of the magnetic field, of TRDs and of the forward cone extended to $\eta = 4$. The configuration numbers refer to table 3.

4.3.1 Results

The doses at cascade maximum in the EM calorimeter as a function of η are reported in table 6 . Computed doses range from 300 Gy/yr near $\eta = 0$ up to 10^5 for $\eta = 4$. Unlike neutron fluxes they depend only on η without any significant influence of the forward cone aperture on values for small rapidities. The effect both of the magnetic field and of the presence of TRDs in the central cavity is small as expected. However it must be pointed out that these data refer to regions were no field was present, while in reality the stray field from the central solenoid can increase such estimates, especially if no iron return yoke is foreseen. These data are in reasonable agreement with previously published estimates[18] of doses in a spherical geometry once the η dependent distance to the EM calorimeter and the geometrical peculiarity of the corner between the Barrel and the End Cap have been taken into account. This conclusion suggests that unlike neutron flux which have been shown to be sensitive also to details, doses can reliably be derived from simple models without the need for complex and CPU expensive simulations in realistic geometries.

Table 6

Dose values (kGy/yr) as a function of rapidity in different LHC detector configurations, at cascade maximum in the EM calorimeter.

Config.	η							
	0.-0.5	0.5-1.	1.-1.5	1.5-2.	2.-2.5	2.5-3.	3.-3.5	3.5-4.
1	.33	.37	.43	.87	4.0	11.	0.	0.
2	.45	.48	.60	1.1	3.8	12.	0.	0.
8	.34	.37	.44	.80	3.6	11.	0.	0.
11	.36	.38	.46	.94	3.6	14.	52.	88.
12	.33	.38	.47	.86	3.8	14.	53.	92.

5. Radiation Environment for a realistic SSC detector

The simplified geometry of the SDC detector used for these calculations is presented in figure 4: the surfaces used for scoring neutron fluxes are also indicated. The Barrel and the End Cap cover the intervals $|\eta| < 1.44$, $1.44 < |\eta| < 3$, starting at R = 210 cm and Z = 420 cm respectively. The Forward Calorimeter goes down

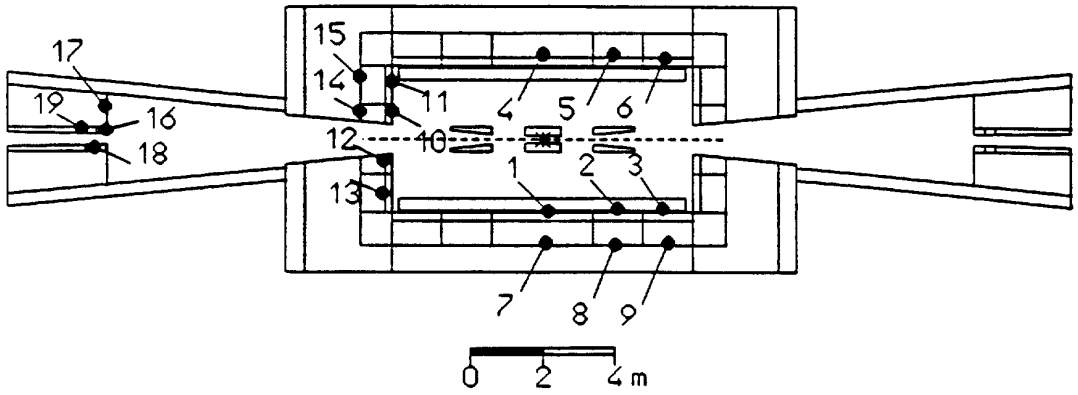

Fig. 4 : Geometry and scoring surfaces used in the calculations for SDC. (horizontal section)

to $\eta = 5$ and starts at Z = 1200 cm. Lead-Scintillator EM and Iron-Scintillator Hadronic Calorimeters have been adopted both for the Barrel and the End Cap. Iron-Lar has been used for the forward Calorimeter. The results of the calculations have been converted to annual doses and fluxes assuming an inelastic cross section $\sigma_{in} = 80\ mb$ and a luminosity of $10^{33} cm^{-2} s^{-1}$ and the same beam time of $10^7\ s$ as for LHC. Systematic uncertainties are similar to the ones presented in section 4.1, but the error associated with the source term should be further increased due to the larger energy and consequent larger uncertainties in the physical model. The results presented in the following have typical statistical errors of 5-10 %. No effort has been made to run a set of configurations like the one shown in table 3, since we believe that most of the conclusions of Section 4 can directly be applied also to the SDC case. Estimates of neutron fluxes and doses for SDC Barrel and End Cap Calorimeters have been already reported and can be compared with the data presented in tables 7 and 8. What is new to our knowledge is the attempt made here to compute fluxes and doses for the Forward Calorimeter.

5.1 Neutron Fluxes

Table 7 presents the annual fluxes computed at the positions shown in fig. 4: runs have been made both with and without the forward Calorimeter, but no detectable difference was found in the results for positions 1 through 15. Neutron fluxes ($E_n > 100$ keV) are well below $10^{12}\ n/cm^2 yr$ in all Barrel positions, reaching 10^{13} roughly in the most exposed position of the End Cap. On the contrary fluxes in the Forward Calorimeter are large and show a strong buildup with depth, going up to 2×10^{14}.

5.2 Dose Rates

Annual Dose rates at cascade maximum are presented in Table 8 as a function of η. Few tens of kGy/yr can be reached in the Forward Calorimeter: this value is about 20 times larger than the maximum dose in the End Cap despite the much

Table 7
Neutron fluxes in SDC(in unit of 10^{12} neutrons/cm^2/yr). Values with statistical errors greater than 20% are marked with an asterisk

Position	1.	2	3	4	5	6	7	8	9	10
Flux, E>100 keV	0.24	0.31	0.38	0.06	0.07	0.08	0.003*	0.004*	0.002*	3.1
Flux, total	1.4	1.6	1.8	0.23	0.31	0.35	0.008*	0.02*	0.005*	6.8

Position	11	12	13	14	15	16	17	18	19
Flux, E>100 keV	0.74	7.5	0.88	2.3	0.26	35.	8.9	197.	182.
Flux, total	2.4	25.	3.7	15.	0.98	67.	25.	332.	338.

Table 8
Dose values (kGy/yr) as a function of rapidity for the SDC detector, at cascade maximum.

	Barrel			End Cap			Forward Calorimeter			
η	0.-0.5	0.5-1.	1.-1.5	1.5-2.	2.-2.5	2.5-3.	3.-3.5	3.5-4.	4.-4.5	4.5-5.
Dose	.016	.019	.020	.11	.50	1.7	.72	2.7	9.8	37.

larger distance from the interaction point.

6. Conclusions

Large systematic errors cannot be avoided in estimating radiation levels for detectors at the future colliders. While the uncertainty on the inelastic cross section is merely a scale factor, more fundamental sources of errors come from the questions still opened about minimum bias events spectra and multiplicities and, with minor importance, the reliability of hadronic cascade simulations. The resulting systematic uncertainty is at least a factor 2: however it has been shown that useful comparisons can be made since most of the systematic effects are the same in every calculation.

Apart from systematic effects, doses can be reliably computed and do not depend too much on details about geometry and composition of the detectors. On the contrary neutron fluxes can be strongly influenced by these factors and require dedicated realistic simulations: there is also evidence that results obtained with simple models can in some cases significantly underestimate the fluxes[19]. The much lower radiation levels of SDC compared with the EAGLE reference Configuration can be only partially explained by the lower luminosity (anyway in part compensated by the higher energy): important effects arise also from the larger Barrel radius, and,

for neutrons only, from the presence of moderating materials in both the EM and Hadronic Calorimeters (to appreciate this last effect look at the difference between EAGLE Config. 1 and 5 in table 5).

7. Acknowledgements

The authors gratefully aknowledge the help given by Prof. J. Ranft, both in running the DTUJET code and with many valuable suggestions and discussions about the modifications of the hadronic part of FLUKA. A special acknowledgement must be given to Mr G. Panini of ENEA-Bologna for the processment and production of the nuclear data sets used for neutron transport, without which the present work would not have been possible. The help given by J. Zazula both in supplying unpublished data and in developing and debugging the FLUKA code is also acknowledged.

8. References

1 P.A. Aarnio, A.Fassò, H.J. Möhring, J. Ranft and G.R. Stevenson, *FLUKA86 user's guide*, CERN TIS-RP/168 (1986), and references therein
2 W.R. Nelson, H. Hirayama and D.W.O. Rogers, SLAC-265 (1985)
3 A. Ferrari, P.R. Sala, R. Guaraldi and F. Padoani *An improved multiple scattering model for charged particle transport*, submitted to *NIM*
4 A. Ferrari and P.R. Sala, *A New MonteCarlo code for inelastic hadron nucleus interactions below 1 GeV*, to be published
5 A. Ferrari and P.R. Sala, *Improvements to the Electromagnetic part of the FLUKA code*, to be published
6 P. Cloth et al., *HERMES user's guide*, KFA-IRE-E (1988) AN/12/88
7 M.B. Emmett, ORNL-4972 (1975)
8 E. Cuccoli, A. Ferrari and G.C. Panini, JEF-DOC-340 (1991)
9 A. Tufail et al., *Phys. ReV.* **D42** (1990) 2187 ; S. Fredriksson et al., *Phys. Rep.* **144** (1987) 187
10 A.M. Kalend et al., *Phys Rev* **C28** (1983) 105
11 J. Ranft, A. Ferrari, P.R. Sala, A. Fassò, G.R. Stevenson and J.M. Zazula, CERN TIS divisional report (1991), to be published
12 A. Fassò et al., CERN TIS-RP/90-19 (1990); J.S. Russ et al., CERN TIS-RP/89-02 (1989)
13 P. Aurence et al.,*Multiparticle Production in a two component dual parton model*, submitted to *Phys. Rev* **D**
14 J. Ranft et al., to be published
15 UA5 Collaboration, G.J. Alner et.al. , CERN-EP/86-213 (1986)
16 J.E. Gover, J.R. Srour, Sandia Report SAND85-0776 (1986)
17 A.M. Ougouag, *IEEE Trans. Nuc. Sci.* **37** (1990) 2219
18 G.R. Stevenson, *proceedings of the Large Hadron Collider Workshop*, CERN 90-10 (1990), vol III pag 566
19 G.R. Stevenson et al., *proceedings of this conference*